Proof-of-Principle of an Energy-Efficient, Iron-Dominated Electromagnet for Physics Experiments

A. Devred, *Senior Member, IEEE*, A. Ballarino, N. Bourcey, F. Mangiarotti, A. Milanese, and C. Petrone

***Abstract*—A number of physics experiments call for the use of iron-dominated, normal-conducting electromagnets to produce moderate fields (2 T range) in a large gap or over a large volume. Although robust and reliable, these magnets require significant electrical power, in the MW range, and can thus be costly to operate, especially in DC mode. We report on the design and test of a superconducting, proof-of-principle demonstrator that makes use of technological developments carried out for the High Luminosity upgrade of the Large Hadron Collider at CERN (HL-LHC). The demonstrator includes a superconducting coil, wound from a MgB_2 cable, and mounted inside an iron yoke with a 62 mm gap. As a first phase, the demonstrator was successfully tested in liquid helium at 4.5 K, generating a magnetic flux density of 1.95 T at a current of 5 kA. In a second phase, currently under preparation, the demonstrator will be tested in gaseous helium at 20 K. The design concepts of the demonstrator can be scaled up to large, iron-dominated electromagnets.**

***Index Terms*—Electromagnet, gaseous helium cooling, HL-LHC, iron-dominated, MgB_2.**

I. Introduction and Motivation

IRON-DOMINATED magnets, where normal-conducting coils generate a magnetic field confined and shaped by the surrounding iron yoke geometry, have been used for many decades in synchrotron accelerators [1], [2], beam transfer lines, and physics experiments [3], [4]. They are relatively straightforward to design and can operate reliably for a long time – some of the CERN normal-conducting magnets have been in operation for over 60 years. They are limited by the iron saturation, which restricts their magnetic flux density range below 1.8–2.0 T. For applications requiring a magnetic field over a large gap or volume, the normal-conducting coils become sizeable and call for significant electrical power in the MW range, which can generate significant operating costs depending on the magnet duty cycle.

Since the Tevatron, and the first large-scale application of low-temperature superconductors in the late 1970s, Nb-Ti and more recently Nb_3Sn magnets have become the workhorses of large physics instruments, with fields up to 14+ T (depending on the applications) and reduced operating costs. However, their major drawback is the requirement of liquid helium cooling and the related cryogenics infrastructure for the low-temperature superconductors.

In the past decade, new opportunities have arisen with the development of superconductors that can be operated at intermediate temperatures and do not require liquid helium cooling.

The High-Luminosity Large Hadron Collider (HL-LHC) project at CERN has promoted several technological developments to improve the performance and reliability of the LHC machine [5]. Among them is an innovative cold powering system [6] to supply current to all HL-LHC Interaction Region magnets [7]. It integrates several circuits in parallel, with lengths exceeding 100 m (including a vertical section of ∼10 m), and relies on a multistage MgB_2 cable, cooled by a forced flow of gaseous helium at temperatures in the 4.5 to 20 K range, and carrying up to ∼130 kA at 25 K [6]. Long lengths of robust, reacted round wire, which were then assembled in large cables, were developed, qualified, industrialized and used for the first time for this project.

MgB_2 technology has gained momentum in the mid-2010s when significantly long tapes started to become available [8]. As often in applied superconductivity, Magnetic Resonance Imaging (MRI) has been a driver, as MgB_2 offers the prospect of developing open systems with simplified cooling [9], [10], [11]. Applying MgB_2 technology to HL-LHC corrector magnets was also promoted by G. Volpini [12], and a sextupole corrector prototype was recently successfully tested at INFN-LASA [13]. Further developments are ongoing on solenoids for high-efficiency klystrons [14], undulators [15], and beam transport magnets [16], [17], as well as on liquid hydrogen cooling [18].

A pioneering work on MgB_2 superferric racetrack magnet was presented in 2008 [19]. This 0.5-m-long magnet, with a 26-mm iron gap, relied on copper-MgB_2 tapes. One of the innovations of the work reported here is the use of a MgB_2 cable made from round wires, thereby enabling higher current intensities for large-scale applications, such as some of the magnets needed for the Search for Hidden Particles (SHiP) experiment under consideration at CERN [20]. After recalling the parameters and performance of the selected MgB_2 cable, we describe the electromagnetic design of the proof-of-principle demonstrator,

Manuscript received 3 October 2023; revised 22 November 2023; accepted 8 December 2023. Date of publication 22 January 2024; date of current version 6 February 2024. *(Corresponding author: A. Devred.)*

The authors are with CERN TE-MSC Group, CH-12 11 Meyrin, Switzerland (e-mail: arnaud.devred@cern.ch).

Color versions of one or more figures in this article are available at https://doi.org/10.1109/TASC.2024.3355872.

Digital Object Identifier 10.1109/TASC.2024.3355872

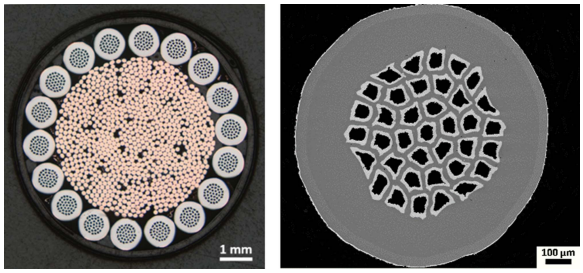

Fig. 1. Cross-sectional views of MgB_2 wire (left) and cable (right) used for the coil of proof-of-principle demonstrator [26].

give some considerations on quench protection, and describe its mechanical design and assembly process. We continue with the results of an initial test in liquid helium at 4.5 K and conclude on the planned next steps.

II. Conductor

One of the critical and long lead items for any superconducting magnet development is the conductor. For the proof-of-principle demonstrator, we selected a MgB_2 cable manufactured and extensively tested for the Superconducting Link of the High Luminosity Large Hadron Collider (HL-LHC) at CERN [6]. The MgB_2 strands were developed by CERN with ASG during the R&D phase of the HL-LHC Superconducting Link [6], [21], [22] and were produced by ASG. They have undergone significant mechanical and electromechanical characterizations [23], [24]. To date, the full quantity of 1450 Km of MgB_2 wire has been produced and successfully qualified. The MgB_2 cable was also developed by CERN [25] and then industrialized, in the framework of HL-LHC WP6a, for production in long lengths by Tratos Cavi, a member of the ICAS consortium.

The MgB_2 wire (Fig. 1(left)) has a diameter of 1 mm. The Monel matrix, into which the superconducting filaments are embedded, incorporates a thin layer of copper plating onto the external surface. The copper is coated with tin-silver to ensure the surface quality of the wire and a controlled electrical resistance among wires when assembled into cables. It also facilitates the realization of low-resistance electrical splices. The cable (Fig. 1(right)) has a nominal diameter of 9.4 mm and consists of eighteen wires, which are twisted around a central stranded copper core with a 4.9-mm diameter. The cable is covered by two layers of tinned copper braids, mostly to provide mechanical stability.

Let us note that, unlike in the case of Nb_3Sn coils that are usually produced with the "wind & react" process, we rely on a "react & wind" process, with the heat treatment required for MgB_2 precipitation applied on-line with wire production prior to cabling. For magnet design and manufacture, it was decided to impose a minimum bending radius of 300 mm on the cable, a value for which it was verified that there is no degradation For reference, the critical bending radius of the wire is 100 mm.

III. Electromagnetic Design

For the electromagnetic design of the demonstrator, we set a target to generate a dipole field up to full iron saturation, in the 1.8–2.0 T range. We then chose a vertical pole gap of 62 mm; a reasonable aperture for a demonstrator, it allows magnetic measurements using already available equipment, and it requires a level of ampere-turns representative of the targeted applications (>100 kA). The pole width was fixed at 180 mm, as a compromise between field quality and achievable flux density.

Although field quality was not a main objective for this demonstrator, it was controlled with side pole shims, but without longitudinal end pole chamfering and with no provision for fine-tuning (after magnetic measurements) via removable end shims. All these measures are well known for normal-conducting magnets and can be readily implemented in the future, especially with a room-temperature yoke. The amount of generated flux is directly linked to the size of the return yoke, which we constrained to the diameter of the largest cryostat in our cryogenic test station (1500 mm).

Another parameter that dictates the overall size is the cable's minimum bending radius of 300 mm. Such a requirement is compatible with its use in large windings, like those needed in spectrometer magnets. It can also be accommodated in this demonstrator using flat racetrack coils.

These considerations led to a design based on an H-type yoke [1], [2]. This layout is more compact and stiffer with respect to a C-type geometry, and in this case is also better suited to house a wide racetrack coil, needed to satisfy the minimum bending radius requirement on the conductor. The overall dimensions of the cross-section are 1282 × 542 mm, for a magnetic length of 1.0 m. The somewhat unusual aspect ratio width/height is related to the specific layout of the coil, with a large bending radius and thus a large inner width with respect to the magnet aperture. Another less conventional choice is the use of a single coil, that is, all the ampere-turns are provided next to one pole, instead of being split evenly across the two. This breaks the typical top/bottom dipolar symmetry, technically allowing odd skew multipole terms in the field expansion, which nevertheless remain small; only the skew quadrupole term in the end region is noticeable. It also introduces a solenoidal component on axis in the ends. Furthermore, the local saturation of the two halves of the yoke is slightly different. These minor drawbacks are more than compensated by the simplicity of having a single coil. Such a choice might also be interesting for the next steps, when the windings will be embedded in a cryostat and the yoke will remain at room temperature. A schematic cross-section with the geometry together with flux lines and intensity (at 5 kA) is shown in Fig. 2.

The coil itself is a double pancake with 2 × 12 turns. The load line is plotted in Fig. 3, alongside reference data for the MgB_2 cable. As this is an iron-dominated design, the peak field on the coil is significantly lower than the field in the aperture. For example, at 5 kA, and considering 2D simulations, we expect 1.85 T in the gap but only 1.08 T maximum on the conductor. The short sample current is estimated to be 9.2 kA and 5.7 kA, at 4.5 K and 20 K, respectively. The Lorentz forces are distributed on the windings along three components: vertical (aligned to the central dipole field), horizontal, and longitudinal. As an order of magnitude, the total vertical force at 5 kA, pushing the coil toward the yoke, is 93 kN.

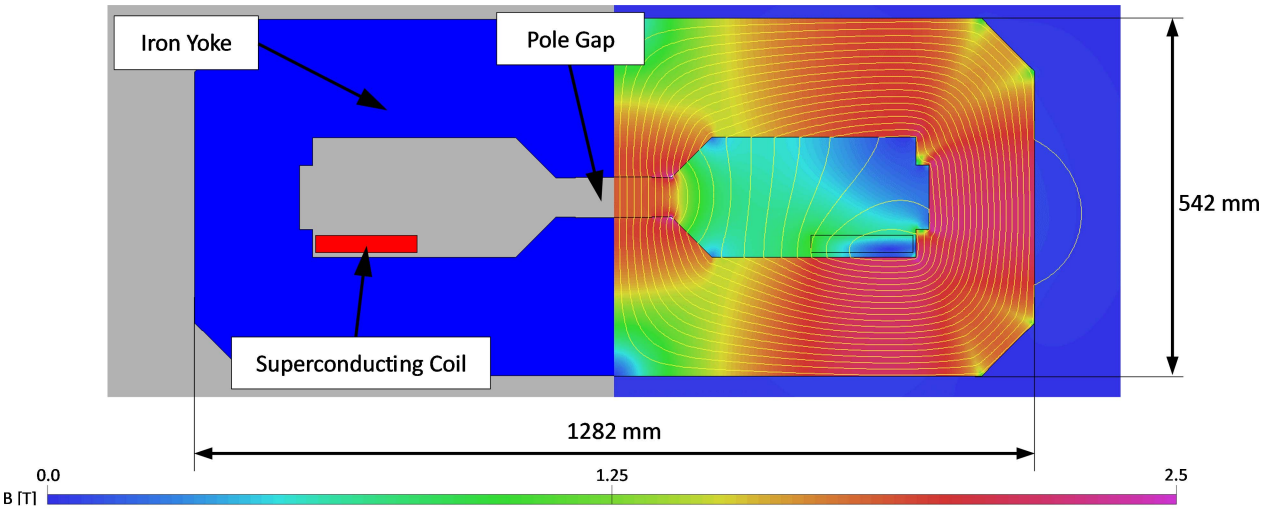

Fig. 2. Electromagnetic model of proof-of-principle demonstrator, with geometry (left) and magnetic flux density lines (right).

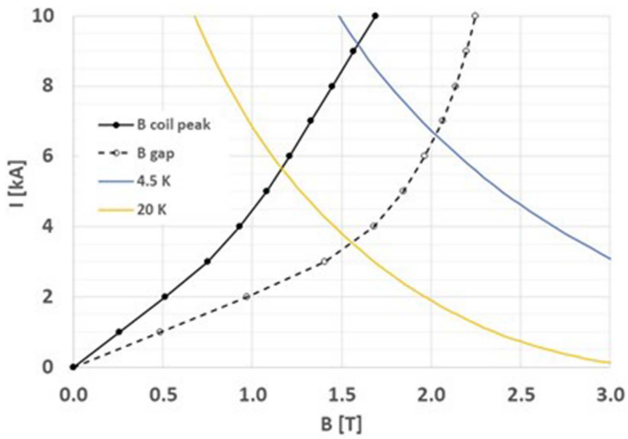

Fig. 3. Magnet load line (2D simulations), with reference data for the MgB_2 cable at 4.5 K and 20 K.

More details on the electromagnetic design, including 2D and 3D simulations, the transfer function, central and integrated field quality, the magnetic field and Lorentz force distribution in the conductor, the impact of different *B-H* curve characteristics, the magnetic energy, and the nonlinear inductance, can be found in [27].

To conclude this part, we estimate at first order the electrical power that would be required with a normal-conducting coil. Keeping all dimensions the same and assuming a round, full (not multi-strand, with a filling factor <1) conductor of 9.4 mm diameter, 5 kA would result in a current density of 72 A/mm^2 on the conductor. Taking the resistivity of copper at room temperature, this would, in turn, translate into 500 kW of power. This high energy consumption for a 1 m long dipole with a 62 mm vertical gap working at 1.85 T, is related to the large current density, that would also pose a severe challenge for cooling. For such a resistive design, a more reasonable assumption for the current density would be $\sim$5 A/mm^2, which would bring the power down to the tens of kW range. However, the coil size would increase by a factor of 15, with a consequent increase in the overall dimensions of the magnet.

IV. Quench Protection

The design goal for the quench detection and magnet protection was to achieve self-protection of the demonstrator magnet at nominal operating conditions at a temperature of 20–25 K, with a transport current of 4–5 kA. The MgB_2 cable incorporates dedicated features required for protection of the HL-LHC superconducting link, including a sizeable amount of copper for stabilization. Also, minimum quench propagation energy and quench-propagation velocity were carefully studied and experimentally validated [28]. This robust cable design was also considered appropriate for use in the demonstrator and a good starting point for future applications in large magnets.

A simplified 1-D quench model was developed for the demonstrator, based on several assumptions: negligible resistance between MgB_2 filaments and the copper matrix, fully adiabatic conditions, and constant quench propagation velocity (v_QP). The assumptions are conservative, save for the fact that the adiabatic conditions may overlook a possible reduction of v_QP due to more efficient cooling in liquid helium. In addition, the inductance of the magnet is assumed constant, and the effects of eddy currents induced in the aluminum formers and the iron yoke are neglected.

Fig. 4 shows the computation results for a quench that occurs at 5 kA and 20 K. The hotspot temperature reaches $\sim$250 K. A sensitivity study was performed on the various unknowns, such as the cable RRR, the v_QP, and the warm circuit parameters. The propagation velocity v_QP was identified as the parameter with the largest impact on the computation results [29].

As illustrated in Fig. 4, a reduction of the propagation velocity by a factor of 10 could yield hotspot temperatures up to 500 K, which could happen during operation in liquid helium at 4.5 K. An energy extraction unit with a 20 mΩ dump resistor was used

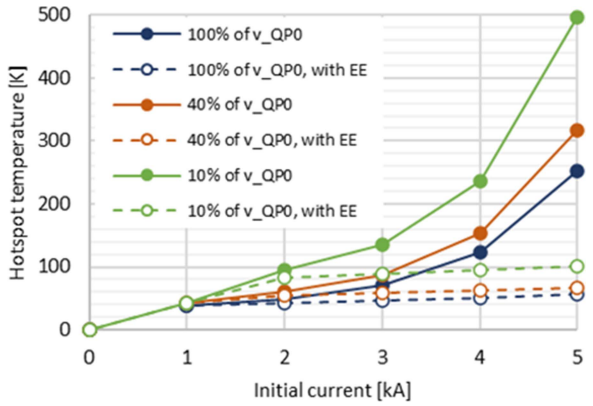

Fig. 4. Expected hotspot temperature as a function of quench current for several values of *v_QP*, expressed as a fraction of the value *v_QP0* measured at 20 K (see [28]). The dashed lines show the expected hotspot temperature using energy extraction as an additional protection system.

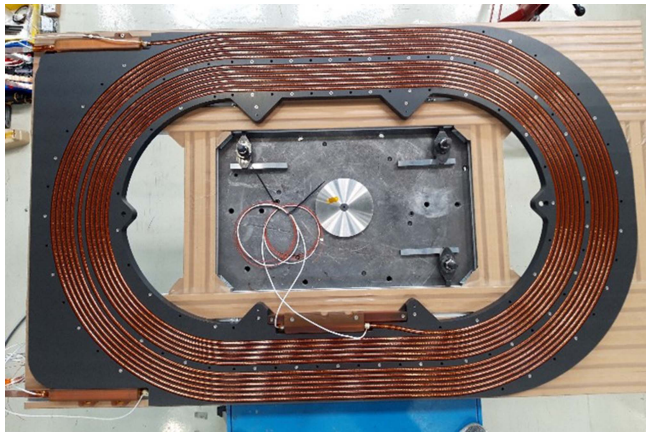

Fig. 5. Top view of the second layer of the coil, with the insulated MgB_2 cable positioned in the grooves of the aluminum former, before placing the cover plate; a pair of voltage taps is placed across the layer jump for monitoring.

to ensure that the hotspot temperature remains below 100 K. The quench detection threshold was set at 10 mV, with a validation window of 5 ms. To obtain more information about quench propagation velocity, the energy extraction trigger was delayed by 300 ms with respect to quench detection and power converter shut off triggers. Further measurements of the quench propagation velocity along this MgB_2 cable in liquid and gaseous helium gas (5–20 K) are planned at a future stage of the project to improve confidence in the model.

V. Mechanical Design and Assembly

The MgB_2 cable was insulated with one layer of 50-μm-thick polyimide, 11 mm wide, wrapped around the cable with a 50% overlap; a winding tension of 12 N was applied to the polyimide tape itself, while no tension was added to the cable. The developed cable length used for winding was 84 m.

The double-pancake coil was wound, without tension, positioning the cable in aluminum alloy (grade 6082) formers, more specifically in half circular grooves, machined precisely to obtain a tight fit with the insulated cable, thus supporting it during powering. The formers were dimensioned to retain the Lorentz forces in the horizontal and longitudinal directions while the vertical component was transmitted to the yoke. Their design was inspired by the radial plates used in the Toroidal Field coils of ITER [30], [31], [32].

The winding of the first layer started from the outermost turn, proceeding inwards; this allowed to avoid a splice in the layer jump. The second former was placed on top, with the reserve spool going through it, and the next layer was wound the other way around, from the layer jump at the inner radius outwards, till the outermost turn. A welding rotating table with a vertical axis was modified to act as a winding machine.

Throughout the manufacturing, we satisfied the requirement of having a minimum bending radius on the cable of 300 mm. The formers were hard anodized to improve the surface hardness while providing some dielectric insulation. The current leads rely on flat Nb–Ti Rutherford-type cables that are spliced to the

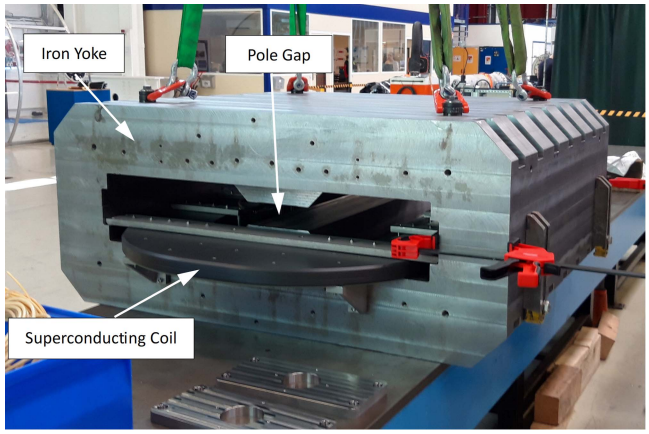

Fig. 6. Demonstrator magnet in the last assembly phase.

MgB_2 cable over a length of 200 mm via resistive soldering with Sn_2Ag, following a design and a process similar to those developed for the HL-LHC superconducting link. Fig. 5 shows a top view of the demonstrator coil.

The iron yoke is made of two symmetric halves, machined using readily available standard construction steel of the S355J2+N grade. The effect on the magnetic performance compared to using a more noble ARMCO iron was computed to be negligible. Furthermore, there was no specific need for high mechanical resistance at cryogenic temperature. Each yoke half has a mass of 2250 kg.

For the final assembly, we aligned the coil in the yoke using two pins, one fixed on the connection side and the other sliding along the longitudinal axis at the other end. This was to avoid thermal stresses arising from differential contractions at cryogenic temperature, particularly between the steel (2.0 mm/m) and the aluminum (4.0 mm/m). A system of clamps and pushers, with interposed G11 shims, was used to properly secure the coil against the yoke. Fig. 6 shows the demonstrator magnet in the final stage of assembly.

At different steps during the fabrication (winding of the first layer, winding of the second layer, completion of the coil, and final assembly), we performed high voltage (500 V) dielectric tests, with no issues.

The above-mentioned fabrication process does not require complex tooling. More specifically, the aim was to avoid a vacuum impregnation step and to guarantee the tight fit groove-to-cable, considering the brittle nature of the conductor.

VI. Test Results

A. Cooldown and Powering

The proof-of-principle demonstrator underwent a first test at the CERN SM18 cryogenic test facility in liquid helium at 4.5 K. The thermal gradients during cooldown and warm-up were limited below 20 K between the inlet and warmest or coldest measurement point in the magnet. After the first cooldown to 4.5 K, the magnet was powered with a ramp rate of 5 A/s to the design current of 5 kA without any natural quench. Then, the magnet was subjected to a thermal cycle to room temperature and, after a second cooldown to 4.5 K, was powered again to 5 kA, with no quench, first at 5 A/s but also at increasing ramp rates, up to 40 A/s. No resistive voltage was observed across the coil. As mentioned above, the magnet was connected to an energy extraction unit to limit hot spot temperature in case of quench. The measured resistance of the splices between MgB_2 and Nb-Ti is 2.6 nΩ, and the measured RRR between 293 K and the critical temperature of 39 K is 38 for both coils (corresponding to a RRR between 273 and 4 K of about 50—this value includes the effect of the Monel which would need to be subtracted to derive the copper RRR).

Provoked triggers of the fast power abort were carried out to validate the quench protection model. As expected, the model is conservative in terms of magnet inductance, as the eddy currents in the structure greatly reduce the effective inductance. Validation of other parameters, such as quench propagation velocity, is expected to be done at a second stage of the project, when operating the magnet at higher temperatures.

B. Magnetic Measurements

For the magnetic measurements, we used an existing rotating-coil magnetometer [33]. The shaft was designed and produced during the HL-LHC prototyping phase and turned out, with its 21.32 mm measuring radius, to be suitable for measuring this demonstrator at approximately 2/3 of the vertical bore. The shaft features seven longitudinal segments, each with three radially mounted induction coils, allowing for a dipole compensation scheme. The 249-mm-long induction coils cover the longitudinal homogeneous field region.

For the magnetic measurement, the magnet was powered using a staircase current cycle, with a ramp rate of 10 A/s and acceleration/deceleration of 1 As^{-2}. A constant current was maintained on the plateaus for four minutes. Figs. 7 and 8 show the measured load lines and the transfer functions in steady-state condition (averaged over 50 seconds on the stabilized plateau) compared to the calculated magnetic field and field integral.

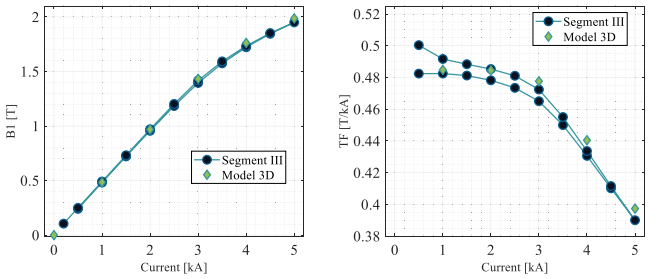

Fig. 7. Dipole field (load line and transfer function) measured by the three central coil segments as a function of the current and compared with expected values from simulations.

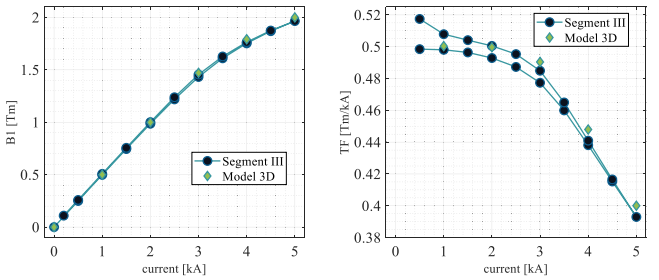

Fig. 8. Integral dipole field (load line and transfer function) measured as a function of the and compared with expected simulation values.

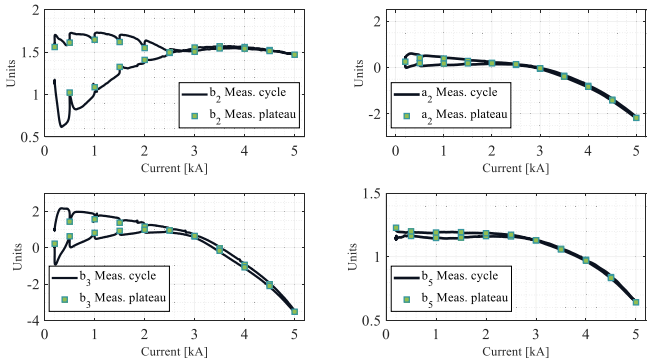

Fig. 9. Normal and skew multipole field components measured by the central segment (III) of the measurement system as a function of current, expressed in units at a reference radius of 20 mm.

The magnet reached a central field of 1.95 T at 5 kA. The measured transfer function agrees with the simulations, with a 2% mismatch at higher currents. This can be explained by the optimistic *B-H* curve used for the yoke (pure iron instead of construction steel). A measurement of the permeability at cryogenic temperature on a representative sample is foreseen. The hysteresis on the load line and transfer function can be attributed to the iron yoke.

The field quality was characterized in terms of circular harmonics. Fig. 9 shows the measured lower-order normal and skew multipole field components as a function of the excitation current at a reference radius of 20 mm. The shaft rotates with a frequency of 1 Hz, and a rotational encoder generates 512 pulses every revolution. The CERN-developed electronic cards (FDI) acquire

TABLE I
NORMAL AND SKEW MULTIPOLE FIELD COMPONENTS AT THE MAGNET CENTER AND AT 20 MM REFERENCE RADIUS

kA	b_2	b_3	b_4	b_5	b_6	a_2	a_3	a_4
1	1.0	1.5	-0.5	1.1	0.2	0.4	0.2	0.4
2	1.4	1.1	-0.5	1.2	0.2	0.2	0.2	0.4
3	1.5	0.6	-0.5	1.1	0.2	0.0	0.1	0.3
4	1.5	-0.9	-0.5	0.9	0.2	-0.8	0.1	0.2
5	1.5	-3.5	-0.5	0.6	0.2	-2.2	0.0	0.0
4	1.5	-1.1	-0.5	0.9	0.2	-0.8	0.1	0.2
3	1.5	0.6	-0.5	1.1	0.2	0.0	0.2	0.4
2	1.5	0.9	-0.5	1.2	0.2	0.2	0.2	0.4
1	1.6	0.8	-0.5	1.2	0.2	0.2	0.1	0.4
AVR	1.5	0.0	-0.5	1.0	0.2	-0.3	0.1	0.3

induced voltage signals with a sampling rate of up to 500 kHz and, based on the trapezoidal rule integration algorithm, evaluate the integral at each external trigger. An analysis of the multipole field components on the staircase plateaus shows a decay time of the order of 50 ss, likely due to eddy currents generated in the aluminum formers and iron yoke during ramping. The maximum width of the hysteresis loop (measured at the end of the decay on the 500 A plateau) is of the order of 10^{-4} for b_3, while it is half of that for b_2 and a_2.

Fig. 9 also shows smooth curves at the beginning and end of each ramp, as low acceleration and deceleration values of the excitation current were required to stabilize the controller response of the power supply. The eddy current effects are not expected to be a problem for spectrometers operating in DC, while the hysteresis loop closes at high current.

Table I lists the low-order multipole field components at a reference radius of 20 mm evaluated in steady-state condition (averaged over the stabilized plateau) for the central part of the magnet. Values for the integrated multipoles are also available and agree with the simulations within one unit range. The unallowed harmonics arise from the asymmetric coil design.

VII. CONCLUSION AND NEXT STEPS

We reported on the design, manufacturing, and test of a proof-of-principle demonstrator for an energy-efficient, iron-dominated magnet relying on a MgB_2 superconducting coil. The 4.5 K tests successfully demonstrated the design concept, both in terms of performance and field quality. This confirms the robustness of the selected MgB_2 cable and its suitability for coil windings in large superferric magnets. It also validates the applicability of a radial-plate-like design to support the winding.

The team is now working with the CERN TE-CRG Group to conduct a test in gaseous helium at 20 K, which is expected in early 2024. Ultimately, the coil will be inserted into a dedicated cryostat to enable its operation at 20 K, while keeping the surrounding iron yoke at room temperature. These phases will be instrumental to confirm the suitability of the design for the proposed application, and they will also allow a full characterization of the heat losses and needed cryogenic power. This is not presented at this preliminary stage as the study is currently ongoing, however we target a factor of at least 100 in the wall plug power, compared to a resistive option.

The design concept and manufacturing process of this demonstrator have been selected to be scalable in a straightforward way to large, iron-dominated electromagnets, such as the ones needed for the Search for Hidden Particles (SHiP) experiment [20]. The design could also be used to retrofit similar existing magnets, by replacing the normal- conducting coils. Moreover, it could be applied to high-temperature superconductor (HTS) cables, such as those developed for the HL-LHC superconducting link [26], [34], thereby opening the possibility of operating at temperatures up to 77 K. However, given the present costs of the conductor and the need for long unit lengths, MgB_2 may remain the most robust and cost-effective option for the time being.

ACKNOWLEDGMENT

The authors acknowledge the important contribution of C. Chatron, for all CAD work, including tooling and integration in the test station, and of S. Luzieux for the cable insulation. The authors are grateful for the support of the CERN EN-MME Group, in particular P. Moyret, for procuring the machined yoke and coil formers. The authors also wish to thank R. Jacobsson, CERN EP-LBD, for inspiring this work, D. Tommasini, formerly CERN TE-MSC, for his exploratory feasibility study, S. Russenschuck for carefully proofreading the manuscript and J.-M. Jimenez, CERN TE Department Head, for his unconditional support for this initiative.

REFERENCES

[1] J. T. Tanabe, *Iron Dominated Electromagnets: design, Fabrication, Assembly and Measurements*. Singapore: World Sci., 2005, doi: 10.1142/5823.
[2] T. Zickler, "Basic design and engineering of normal-conducting, iron-dominated electromagnets," 2011, *arXiv:1103.1119*.
[3] D. Swoboda, L. Leistam, L. Pigni, D. Cacaut, E. Kochournikov, and A. Vodopianov, "Status of the ALICE magnet system," *IEEE Trans. Appl. Supercond.*, vol. 12, no. 1, pp. 432–437, Mar. 2002.
[4] J. Andre, W. Flegel, P. A. Giudici, O. Jamet, and M. Losasso, "Status of the LHCb dipole magnet," *IEEE Trans. Appl. Supercond.*, vol. 14, no. 2, pp. 509–513, Jun. 2004.
[5] O. Brüning and L. Rossi, Ed. *The High Luminosity Large Hadron Collider* (Advances Series on Directions in Energy Physics), vol. 24. Singapore: World Sci., 2015.
[6] A. Ballarino, "Development of superconducting links for the large hadron machine," *Supercond. Sci. Technol.*, vol. 27, 2014, Art. no. 044024.
[7] E. Todesco et al., "The high luminosity LHC interaction region magnets towards series production," *Supercond. Sci. Technol.*, vol. 34, 2021, Art. no. 053001.
[8] R. Flükiger, Ed. *MgB_2 Superconducting Wires: Basics and Applications* (World Scientific Series in Applications of Superconductivity Related Phenomena), vol. 2. Singapore: World Sci., 2016.
[9] M. Razeti et al., "Construction and operation of cryogen free MgB_2 magnets for open MRI system," *IEEE Trans. Appl. Supercond.*, vol. 18, no. 2, pp. 882–886, Jun. 2008.
[10] T. Baig et al., "Conceptual designs of conduction cooled MgB_2 magnets for 1.5 and 3.0 T full body MRI systems," *Supercond. Sci. Technol.*, vol. 30, 2017, Art. no. 043002.
[11] Hitachi Ltd. Brochure. [Online]. Available: https://www.hitachi.com/rd/news/topics/2021/0301.html
[12] G. Volpini, J. Rysti, and M. Statera, "Electromagnetic study of a round coil superferric magnet," *IEEE Trans. Appl. Supercond.*, vol. 26, no. 4, Jun. 2016, Art. no. 4103505.
[13] S. Mariotto et al., "Performances of the first full-length module prototype of the MgB_2 round coil superferric magnet at LASA," *IEEE Trans. Appl. Supercond.*, vol. 33, no. 5, Aug. 2023, Art. no. 4002505.
[14] A. Yamamoto et al., "Applying superconducting magnet technology for high-efficiency klystrons in particle accelerator RF systems," *IEEE Trans. Appl. Supercond.*, vol. 30, no. 4, Jun. 2020, Art. no. 4101304.

[15] T. Tanabe and V. Smaluk, "Advantage of superconducting device using 26 MgB_2 wires," Brookhaven Nat. Lab., Upton, NY, USA, Tech. Rep. NSLSII-ASD-TN-347; BNL-221237-2021-TECH, 2022.
[16] K. Melconian et al., "Design and development of a MgB_2-based sector dipole and beam transport channel for a strong-focusing cyclotron," *AIP Conf. Proc.*, vol. 1573, pp. 739–745, 2014.
[17] L. Rossi, S. Mariotto, and S. Sorti, "Energy saving magnets for beam lines," in *Proc. 14th Int. Part. Accel. Conf.*, 2023.
[18] Y. Iwami et al., "Excitation characteristics of MgB_2 race-track coil immersed in liquid hydrogen," *J. Phys.: Conf. Ser.*, vol. 1559, 2020, Art. no. 012147.
[19] R. Musenich et al., "A MgB_2 superferric racetrack magnet," *Supercond. Sci. Technol.*, vol. 21, 2008, Art. no. 105014.
[20] C. Ahdida et al., "The SHiP experiment at the proposed CERN SPS beam dump facility," *Eur. Phys. J. C*, vol. 82, 2022, Art. no. 486.
[21] A. Ballarino and R. Flükiger, "Status of MgB_2 wire and cable applications in Europe," *J. Phys.: Conf. Ser.*, vol. 871, 2017, Art. no. 012098.
[22] A. Ballarino, B. Bordini, and S. Giannelli, "MgB_2 transmission lines for the large hadron collider," in *MgB_2 Superconducting Wires: Basics and Applications* (World Scientific Series in Applications of Superconductivity Related Phenomena), Bristol, U.K.: IOP Publishing, 2016, ch. 6D, pp. 581–591.
[23] M. Sugano, A. Ballarino, B. Bartova, R. Bjoerstad, C. Scheuerlein, and G. Grasso, "Characterization of mechanical properties of MgB_2 conductor for the superconductor link project at CERN," *IEEE Trans. Appl. Supercond.*, vol. 25, no. 3, Jun. 2015, Art. no. 4801004.
[24] K. Konstantopoulou et al., "Electro-mechanical characterization of MgB_2 wires for the superconducting link project at CERN," *Supercond. Sci. Technol.*, vol. 29, 2016, Art. no. 084005.
[25] K. Konstantopoulou et al., "Design optimization evaluation of the 3 kA MgB_2 cable at 4.3 K for the superconducting link project at CERN," *Supercond. Sci. Technol.*, vol. 32, 2019, Art. no. 085003.
[26] A. Ballarino, "New superconducting technologies for the HL-LHC and beyond," *CERN Courier*, vol. 63, no. 3, pp. 37–41, May/Jun. 2023.
[27] A. Milanese, "Magnetic design of a superferric MgB_2 demonstrator," CERN TE-MSC Internal Note, EDMS: 2939566, 2023.
[28] S. Gianelli, G. Montenero, and A. Ballarino, "Quench propagation in helium-gas-cooled MgB_2 cables," *IEEE Trans. Appl. Supercond.*, vol. 26, no. 3, Apr. 2016, Art. no. 5400705.
[29] F. Mangiarotti, "Quench protection studies of a superferric MgB_2 dipole demonstrator," CERN TE-MSC Internal Note, EDMS: 2939340, 2023.
[30] R. Maix et al., "Manufacture of the ITER TF model coil," in *Proc. 20th Symp. Fusion Technol.*, 1998, Art. no. 833.
[31] K. Abe et al., "Manufacturing study and trial fabrication of radial plate for ITER toroidal field coil," *IEEE Trans. Appl. Supercond.*, vol. 16, no. 2, pp. 807–810, Jun. 2006.
[32] E. Boter et al., "F4E procurement of radial plates for the EU ITER TF coils," *IEEE Trans. Appl. Supercond.*, vol. 26, no. 4, Jun. 2016, Art. no. 4203804.
[33] L. Fiscarelli et al., "Magnetic measurements and analysis of the first 11-T Nb_3Sn dipole models developed at CERN for HL-LHC," *IEEE Trans. Appl. Supercond.*, vol. 26, no. 4, Jun. 2016, Art. no. 4003805.
[34] C. Barth, M.-P. Careil, A. C. Zurita, J. Fleiter, and A. Ballarino, "Development, construction and commissioning of a fully automated cabling machine for round multi-layer REBCO cables," *IEEE Trans. Appl. Supercond.*, vol. 33, no. 5, Aug. 2023, Art. no. 4801707.